

# Turbulent behavior of a fine mesh ( $1/12^\circ$ ) numerical simulation of the North Atlantic

A.M. Paiva <sup>\*</sup>, J.T. Hargrove, E.P. Chassignet, R. Bleck

*Division of Meteorology and Physical Oceanography, Rosenstiel School of Marine and Atmospheric Science, University of Miami, 4600 Rickenbacker Causeway, Miami, FL 33149, USA*

Received 14 November 1997; accepted 15 May 1998

---

## Abstract

The geostrophic turbulent behavior of a fine mesh ( $1/12^\circ$ ) numerical simulation of the North Atlantic is discussed and compared to observations and coarser numerical simulations. The Miami Isopycnic Coordinate Ocean Model (MICOM) was configured for the North and Equatorial Atlantic ( $28^\circ\text{S}$ – $65^\circ\text{N}$ ) with a horizontal resolution of  $1/12^\circ$  (average mesh size on the order of 6 km) and 16 layers in the vertical. Such a set-up demands the latest in high performance computing. The unique aspects of this simulation are (a) a correct Gulf Stream separation from the North American coast and (b) high eddy activity. These results support the view that an inertial boundary layer (which results from the fine resolution) is an important factor in the separation process and that resolution of the first Rossby radius of deformation is necessary for a correct representation of baroclinic instabilities. Sea surface height variability spectra are computed from the model results and compared to observations and previous models, within the framework of the geostrophic turbulence theory. Length scales representative of the simulated eddy field compare well with observations based on altimeter data. Despite higher eddy activity, there is no significant geographic variation in spectral slope in the inertial ranges consistent with previous simulations with coarser resolution. Observations, on the other hand, show a flattening in the spectra derived from altimeter data in weakly energetic areas when compared to spectra from highly energetic areas of the Atlantic. The possible impact of mechanisms not represented in the model, such as high frequency and high wave number wind forcing, is then discussed. © 1999 Elsevier Science B.V. All rights reserved.

*Keywords:* turbulent behavior; fine mesh ( $1/12^\circ$ ) numerical simulation; North Atlantic; Equatorial Atlantic; Miami Isopycnic Coordinate Ocean Model (MICOM)

---

## 1. Introduction

The constraints of both energy and enstrophy (mean square vorticity) conservation in two-dimensional turbulent flows lead to the existence of two

inertial subranges, characterized by the transfer of energy towards lower wave numbers and of enstrophy toward higher wave numbers (Kraichnan, 1967). Dimensional arguments applied to the kinetic energy wave number spectrum yield a  $k^{-5/3}$  slope for the inverse energy cascade and a  $k^{-3}$  slope for the forward enstrophy cascade. This result is strikingly different from the transfer of energy towards smaller scales observed in three-dimensional turbulence as

---

<sup>\*</sup> Corresponding author. Fax: +1-305-361-46-96; E-mail: paiva@idefix.rsmas.miami.edu

described by the well known Kolmogorov's law, and is a direct consequence of enstrophy conservation.

Kraichnan's hypothesis is important for its applicability to the study of the variability of large scale geophysical flows, which are approximately two-dimensional due to the small ratio of vertical to horizontal scales and the effects of earth's rotation and vertical stratification. Charney (1971) and Hua and Haidvogel (1986) showed that the  $k^{-3}$  law holds for three-dimensional quasi-geostrophic flows, providing a theoretical framework for explaining observational

and model results of atmospheric and oceanic turbulence.

The computation of wave number spectra associated with the mesoscale variability of the large scale ocean circulation was made possible by the advent of sea surface height (SSH) data derived from satellite altimeter measurements. Fu (1983) suggested that the  $k^{-3}$  law for the kinetic energy spectrum is equivalent to a  $k^{-5}$  law for the SSH variability through the geostrophic relationship. Using SEASAT altimeter data, he computed wave number spectra for various

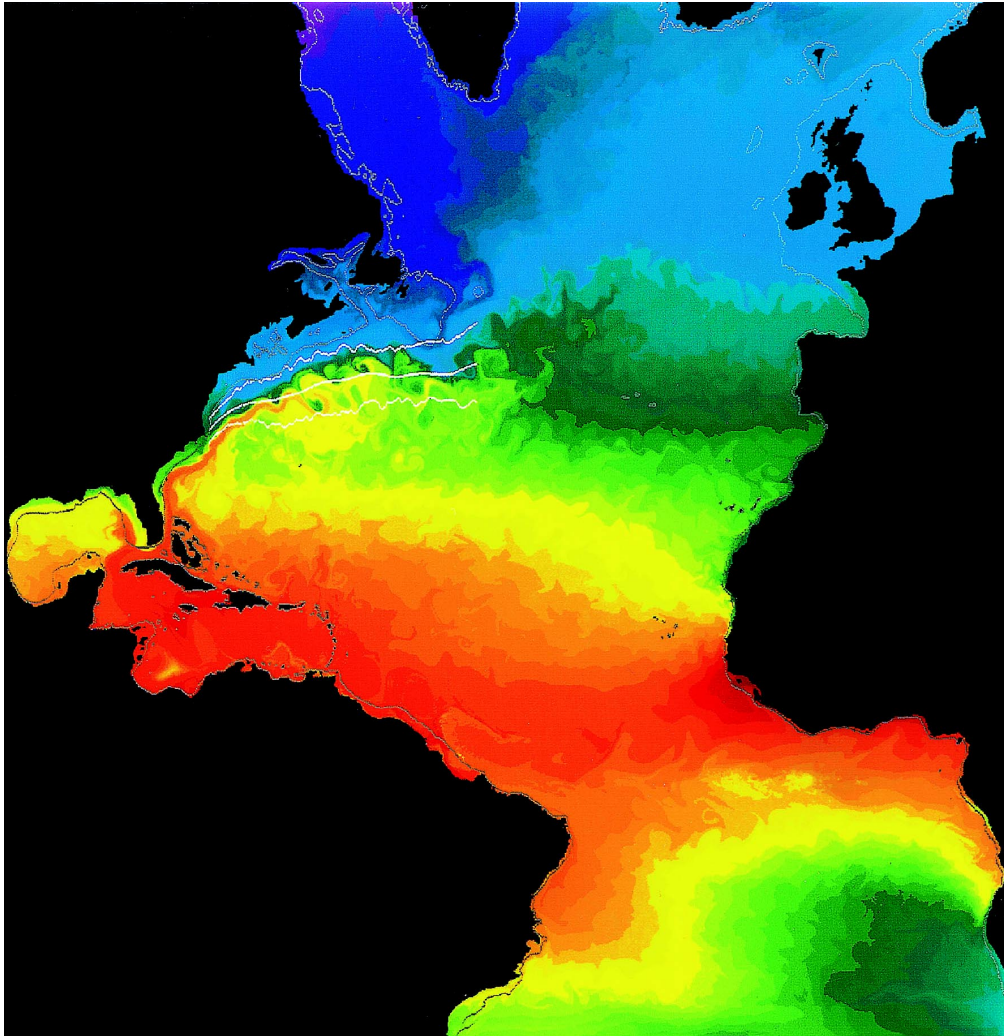


Fig. 1. Snapshot of model SST field in November of year 6 (warmer hues denote warmer temperatures). Dotted line represents mean position of the Gulf Stream and solid lines its northward and southward limits, based on satellite data (courtesy of A. Mariano and M. Chin).

regions of the world ocean, finding that highly energetic areas close to western boundary currents exhibited  $k^{-5}$  slopes, but that the more quiescent eastern oceanic basins presented much weaker slopes, close to  $k^{-1}$ . Subsequent observations based on GEOSAT altimeter data for the North Atlantic (Le Traon et al., 1990; hereafter, LT) and the South Atlantic (Forbes et al., 1993) showed spectral slopes varying consistently from  $k^{-4}$  to  $k^{-2}$  from the western to the eastern part of the domain.

It has been argued that the decrease in spectral slope reflects different dynamical regimes, with barotropic and baroclinic instabilities as the main source of variability in the western part of the domain and wind fluctuations and topographic interactions dictating the behavior in the eastern part of the domain (LT; Le Traon, 1993). A second view, suggested by Stammer and Böning (1993; hereafter, SB), states that the differences in spectral slopes are due to the contamination of the signal by instrument noise in the less energetic eastern basins. In their

analysis of a medium resolution numerical simulation of the North Atlantic ( $1/3^\circ$  by  $2/5^\circ$ ), SB found spectral slopes uniform throughout the model domain. However, the model configuration used by SB was only marginally eddy resolving and the modeled Gulf Stream overshoots the separation point at Cape Hatteras, resulting in a more northward path than that seen in observations.

In this paper, we describe the SSH mesoscale variability of a fine mesh ( $1/12^\circ$ ) numerical simulation of the North Atlantic performed with the Miami Isopycnic Coordinate Ocean Model—MICOM (Bleck and Chassignet, 1994). At this resolution, the model is fully eddy resolving (average mesh size on the order of 6 km) and produces a very inertial Gulf Stream that separates from the coast at Cape Hatteras and follows a path that is within the observed range (Figs. 1 and 2). Sea surface height variability spectra and statistical length scales of the eddy field are computed from the model results and compared to observations and previous model simulations. Since

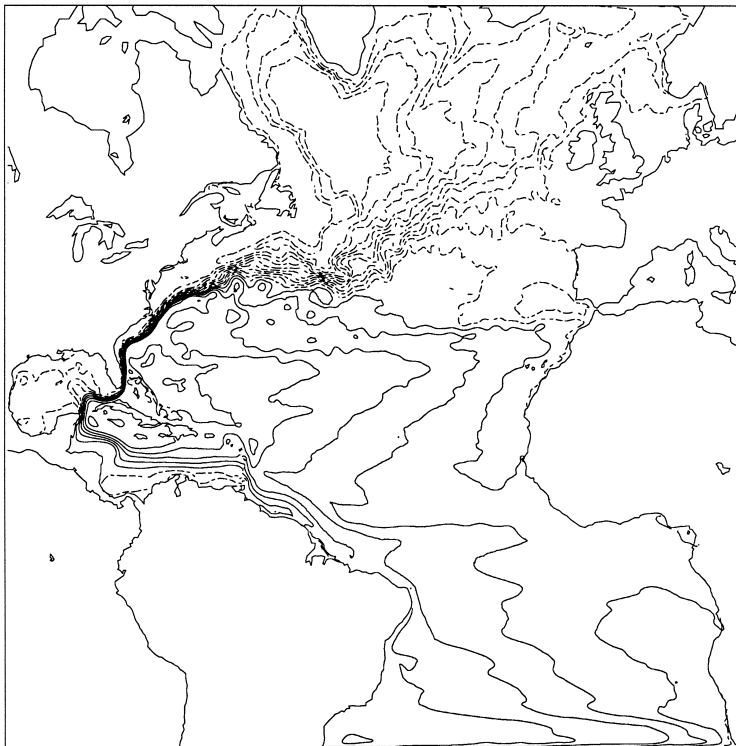


Fig. 2. Model mean sea surface height. Solid lines indicate positive values. Contour interval is 10 cm.

a significant part of the oceanic mesoscale variability in the North Atlantic is associated with eddy activity generated by the Gulf Stream, it is important to determine if an improved separation and higher eddy activity affect the simulated turbulent behavior. Statistics of the eddy field as derived from altimeter data provide important information against which one can check the model solutions (Chao and Fu, 1996). Model results can also help in the interpretation of observational data (Le Traon, 1993).

## 2. Model configuration

The MICOM is well documented in the literature. For a review, the reader is referred to the works of Bleck et al. (1992) and Bleck and Chassignet (1994). The fundamental reason for modeling ocean flow in density coordinates is that this system suppresses the ‘diapycnal’ component of numerically caused dispersion of material and thermodynamic properties (temperature, salinity, ...). This characteristic allows isopycnal models to keep the deep water masses from warming up, as has been shown to occur in models framed in Cartesian coordinates (Chassignet et al., 1996). Furthermore, the association of vertical

shear with isopycnal packing and tilting in the ocean makes isopycnal models appropriate for studies of strong baroclinic currents such as the Gulf Stream.

The computational domain is the North and Equatorial Atlantic Ocean basin from 28°S to 65°N, including the Caribbean Sea and the Gulf of Mexico (Fig. 1). The bottom topography is derived from a digital terrain data set with 5' latitude–longitude resolution (ETOPO5). The surface boundary conditions are based on the COADS monthly climatological data sets (da Silva et al., 1994). Open ocean boundaries are treated as closed, but are outfitted with 3° buffer zones in which temperature  $T$  and salinity  $S$  are linearly relaxed toward their seasonally varying climatological values (Levitus, 1982). These buffer zones restore the  $T$  and  $S$  fields to climatology in order to approximately recover the vertical shear of the currents through geostrophic adjustment. The restoring time scale varies from 30 days at the inner edge, linearly decreasing to 5 days at the walls.

The horizontal grid is defined on a Mercator projection with resolution given by  $1/12^\circ \times 1/12^\circ \cos(\phi)$ , where  $\phi$  is the latitude. The vertical density structure is represented by 15 isopycnal layers, topped by an active surface mixed layer. The vertical grid was chosen to provide maximum resolution in the

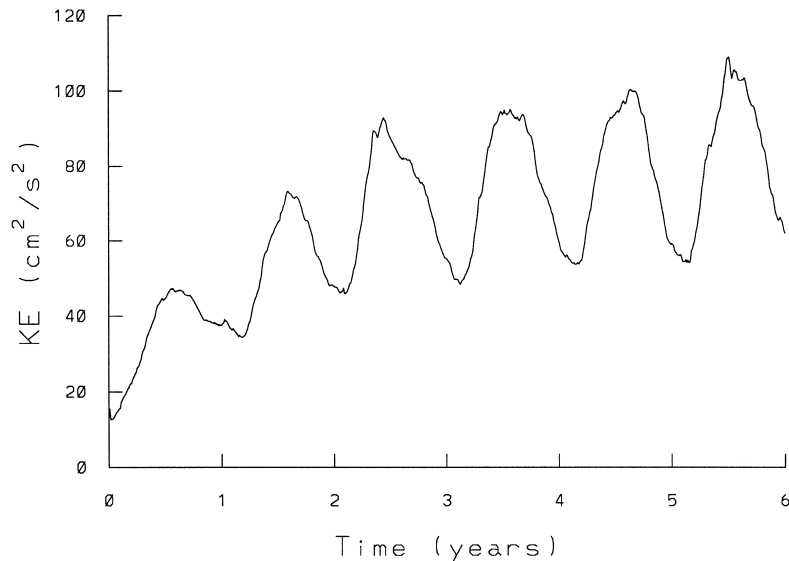


Fig. 3. Time evolution of the model surface kinetic energy per unit mass.

upper part of the ocean. The computational requirements for basin-scale ocean modeling at this resolution are extreme and demand the latest in high performance computing (Bleck et al., 1995). The model was spun up from rest and is presently in its 6th year of integration. While the baroclinic structure is still evolving, the upper circulation is approaching equilibrium as illustrated by the time evolution of the surface kinetic energy (Fig. 3), allowing for investigation of the surface eddy fields. The simulation is being carried out on a 512-processor Cray T3E at the Pittsburgh Supercomputer Center.

### 3. Results

The increase in resolution drastically altered the model's behavior in comparison to previous coarse-resolution simulations. The major differences are (a) a correct Gulf Stream separation and (b) higher eddy activity. These results support the view that an inertial boundary layer, which results from the fine resolution, is an important factor in the separation process (Özgökmen et al., 1997) and that resolution of the first Rossby radius of deformation is necessary for a correct representation of baroclinic instabilities. The simulated Gulf Stream is highly inertial, meanders strongly, and sheds several cyclonic and anti-cyclonic rings. Similar improvements in the Gulf Stream separation were also observed with a geopotential coordinate model by Chao et al. (1996) and Smith et al. (1998) when the resolution was increased to  $1/6^\circ$  and  $1/10^\circ$ , respectively.

The model rms (root mean square) SSH variability is computed by subtracting the spatially dependent time-mean field (Fig. 2) from the instantaneous fields and is shown in Fig. 4a. The rms SSH variability derived from the TOPEX/Poseidon measurements over the same domain area is presented for comparison in Fig. 4b. The model captures most of the major features present in the observations. The maximum variability occurs in the Gulf Stream, where the SSH variability exceeds 30 cm. In both the observations and the model results, the enhanced variability in the subpolar gyre is mostly associated with the North Atlantic Current. In the subtropical gyre, the number of rings shed from the North Brazil Current is higher in the numerical simulation than in

the observations. Consequently, the model SSH rms values are stronger in that region. The Azores current is a robust feature in the model simulation and, as in the TOPEX/Poseidon data, is an important source of variability in the eastern subtropical gyre. In the weakly energetic areas of the northern and eastern parts of the domain, however, the model variability is underestimated compared to altimetry.

For the purpose of the spectral calculations, the SSH of the last 2 years of the simulation was sampled every 10 days and the domain was divided into 10 by  $10^\circ$  boxes extending from  $20^\circ\text{S}$  to  $60^\circ\text{N}$  and  $10^\circ\text{E}$  to  $70^\circ\text{W}$  (Fig. 5). The configuration and position of the boxes are arbitrary in the sense that they were not chosen from an a priori knowledge of areas of distinct dynamical regimes. This allows for a regular mapping of most of the domain and direct comparisons to previous results such as those of LT and SB. The size of the boxes restricts the analysis to wavelengths of scales up to approximately 1000 km. The time averaged spectra are computed in each box as they are from the observations, except that the ascending and descending tracks of the satellite data are the grid latitude and longitude lines in the model. A cosine taper window is applied to the first and last 10% of each line segment, and the spectra are calculated using a Fast Fourier Transform. The number of degrees of freedom of the spectral estimation is computed as in LT by assuming that the line segments are independent if separated by a length scale of 300 km and a time scale of 50 days. This results in more than 100 degrees of freedom per box. Averaging all latitudinal and longitudinal spectra within each box to generate a single spectrum representative of each subdomain is justified by the fact that the differences between the longitudinal and latitudinal spectra are small for most of the subdomains, suggesting isotropy of the SSH field. This is illustrated by the upper and middle curves in Fig. 6, which compares latitudinal and longitudinal spectra computed for boxes 35N and 50N. Larger differences, still within the 95% confidence intervals, may be found for longer wavelengths in some subdomains, although these do not affect the spectral slopes and peak wavelengths. The same assumption of isotropy is made when the spectra from ascending and descending satellite tracks are averaged in the observations. Significant differences are observed for long

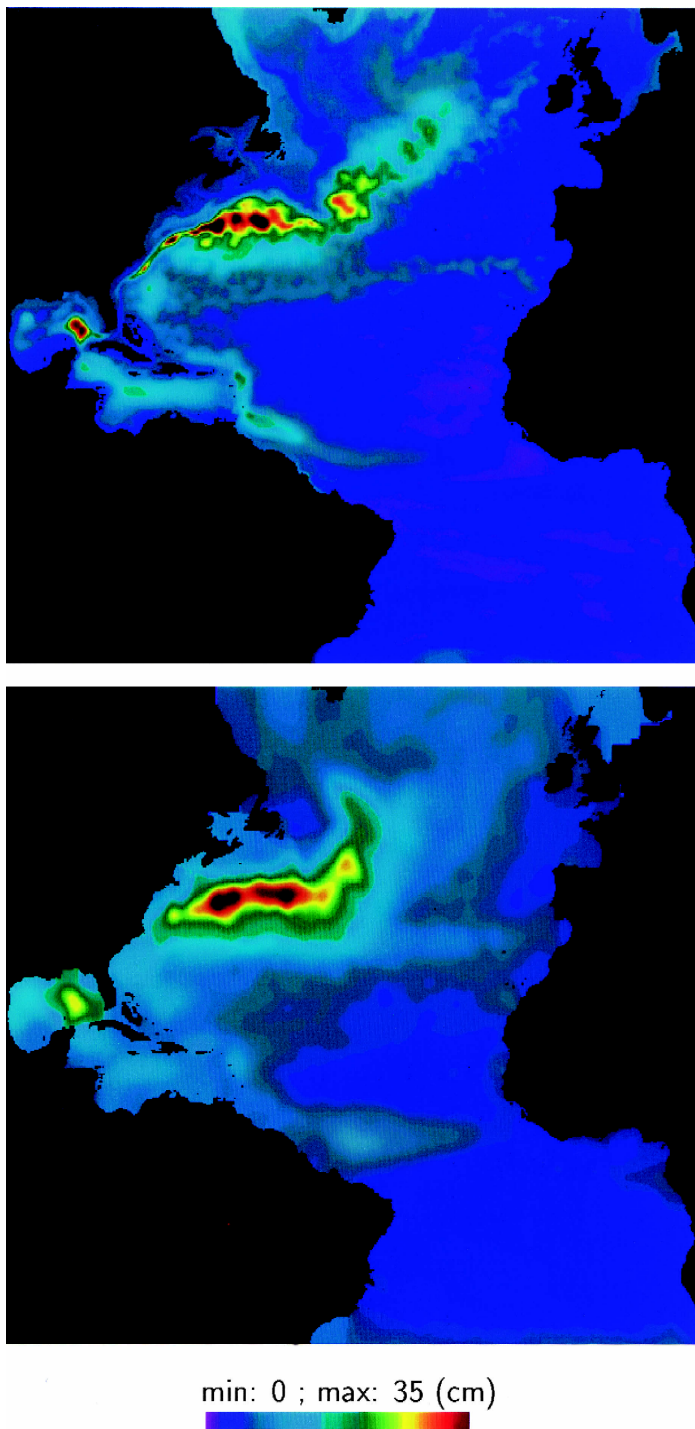


Fig. 4. Sea surface height variability (in cm) from (a, above) the last 3 years of the high-resolution MICOM simulation and (b, below) TOPEX/Poseidon (courtesy of NASA/JPL; provided by O. Brown and G. Goni).

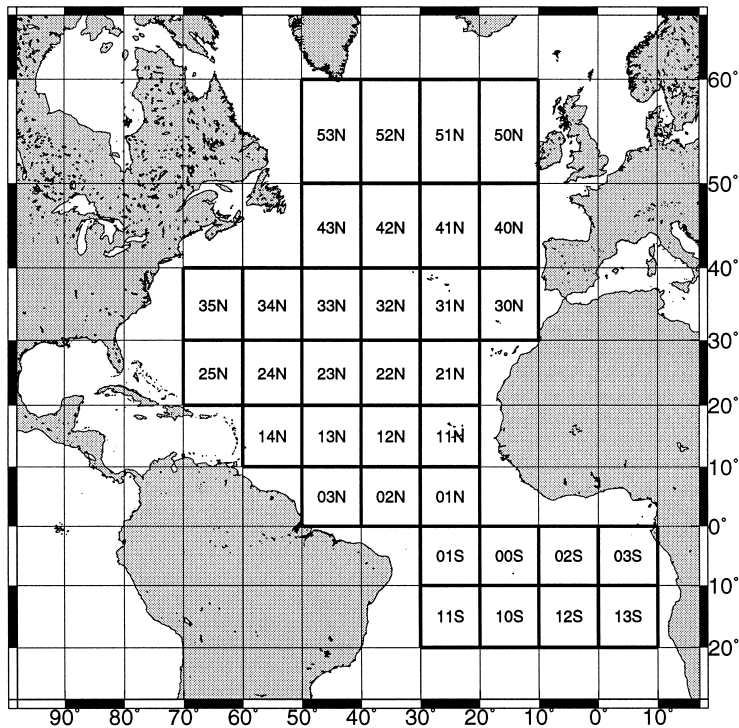


Fig. 5. Limits of subdomains for spectral computations.

wavelengths in some subdomains in the South Atlantic, as illustrated by the bottom curves in Fig. 6.

The spectra for the various subregions are presented in Fig. 7, grouped by latitude. As in the satellite data, most spectra present a plateau at long wavelengths followed by a range of well defined negative slope from around 500 km to 100 km. For wavelengths shorter than about 100 km, spectra based on altimeter data flatten and eventually whiten. This noise floor is not present in the model results; the model energy levels are much lower at these scales and decrease monotonically with wavelength. When contrasted with the observations of LT, all the model spectra exhibit lower energy levels.

The wave number at which the peak in spectral energy occurs increases with latitude (equivalent to a poleward decrease in wavelength). Energy peaks are not well defined south of 10°N. The zonally averaged peak wavelengths ( $l_m$ ) are approximately 500 km from 10 to 30°N, 400 km from 30 to 40°N, and 300 km from 40 to 50°N, in good agreement with the

GEOSAT results of LT. From 50 to 60°N, the peak wavelength is around 280 km, which is somewhat higher than the 200 km estimated from observations (LT). For latitudes up to 50°N, the spectral slopes do not differ much from  $k^{-4}$  (a  $k^{-4}$  slope line is included in Fig. 7 for comparison). This result is consistent with the numerical results of SB, although in contrast with the results of LT based on GEOSAT. North of 50°N, the slopes are consistently smaller than  $k^{-4}$ .

Frequency ( $f$ ) spectra were also computed for each box. A strong signal at the annual period is present in all subdomains. Lower latitude regions also have pronounced energy in the subannual period with a weaker signal at higher latitudes. This is illustrated in the three lowermost curves of Fig. 8 (in order of increasing energy), which represent the frequency spectra for boxes 11N, 31N and 51N, respectively. The spectra for the high energetic subdomains over the Gulf Stream region are very similar and show a  $f^{-2}$  dependence for periods shorter

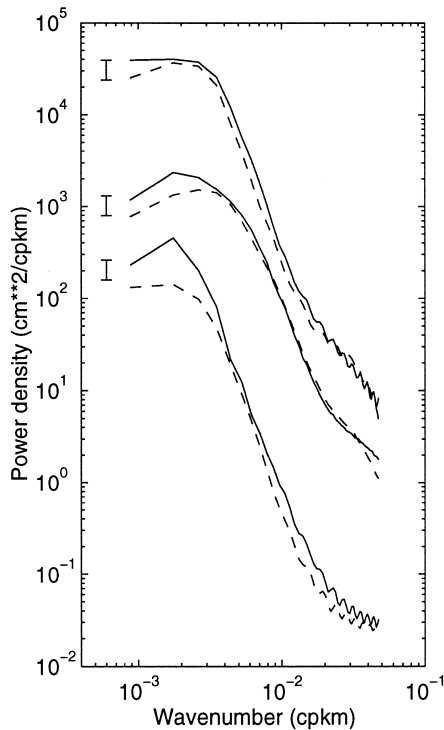


Fig. 6. Comparison of longitudinal (solid line) and latitudinal (dashed line) wave number spectra for boxes 35N (upper curves), 50N (middle curves) and 10S (lower curves). Vertical lines are the 95% interval.

than 100 days (uppermost curves in Fig. 8) in agreement with observations (Stammer and Böning, 1996; Blayo et al., 1996).

## 4. Discussion

### 4.1. Spatial scales

The decrease in wavelength ( $l_m$ ) of maximum spectral energy with latitude is consistent with baroclinic instability theory, in which the wavelength of the most unstable wave is related to the first baroclinic Rossby radius of deformation ( $R_d$ ). This decrease is also consistent with observations (LT). The behavior at latitudes higher than 50°N where  $l_m \approx 300$  km (especially box 53N where  $l_m \approx 400$  km) is somewhat anomalous since these scales are more typical at lower latitudes (either 40 to 50°N or 30 to 40°N). For latitudes higher than 50°N, the model

resolution (around 5 km) is only marginally eddy resolving when compared to an observed Rossby radius of deformation  $R_d$  of about 9 km (Emery et al., 1984). At these latitudes, the model may not be able to represent accurately the baroclinic instability process. In addition, the fluid column is not as stratified and the associated flows are less baroclinic, thus leading to an increase in spatial scales (Stammer, 1997). This factor may be enhanced in the model in regions of deep mixed layer such as in the western subpolar gyre (i.e., box 53N).

Another method of characterizing the length scales of the SSH eddy field, which has been applied to both GEOSAT and TOPEX/Poseidon (LT; SB; Stammer, 1997), is through the autocovariance function  $C(s)$ , computed by the inverse Fourier Transform of the wave number spectra. A decorrelation length scale ( $L_0$ ) can be defined as the lag of the first zero crossing of the autocorrelation function  $C(s)/C(0)$ . Associated integral scales can also be defined as:

$$L_1 = \frac{1}{C(0)} \int_0^{L_0} C(s) ds \quad (1)$$

and

$$L_2 = \frac{1}{C^2(0)} \int_0^{L_{\max}} C^2(s) ds. \quad (2)$$

The latitudinal dependence of the zonally averaged values of  $L_0$ ,  $L_1$ , and  $L_2$  derived from the model data is shown in Fig. 9. The overall distribution, with higher values at the equatorial region and lower at higher latitudes, agrees well with the results of SB. The absolute values cannot be directly compared to SB since our data were detrended prior to the computation. The distribution compares well, however, with the  $L_0$  spatial distribution of the detrended altimeter data for the North Atlantic as presented by Stammer (1997, Fig. 21a). The values based on TOPEX/Poseidon vary from around 180 km at the equator to around 80 km at 60°N, very similar to the model results. The  $L_0$  value for the northernmost latitude band is overestimated in the model for the reasons discussed previously.

Analyzing the GEOSAT data, SB showed a linear relationship between the lag of the first zero crossing and the Rossby radius of deformation for latitudes

poleward of  $10^\circ$ . For the detrended TOPEX/Poseidon data in the Atlantic, Stammer (1997) found the relation  $L_0 = 0.7R_d + 88$  km. The values of  $L_0$  and  $L_1$  computed in each box for the model results are plotted in Fig. 10 against the values of  $R_d$  computed by Emery et al. (1984). As in SB, a linear dependence is suggested for latitudes northward of  $10^\circ\text{N}$ . For this region we obtained  $L_0 = 0.85R_d + 86$ , which compares well to the relationship based on the altimeter data. For the integral scales we obtained  $L_1 = 0.51R_d + 48$  and  $L_2 = 0.53R_d + 40$ .

#### 4.2. Spectral slopes

The question of whether Kraichnan's theory is applicable to the real ocean and realistic numerical simulations is complicated by several factors. The two theoretical inertial ranges have been reproduced in numerical experiments under controlled conditions, namely with energy input occurring at a single wave number (Lilly, 1969). In the ocean, however, the main source of eddy energy is barotropic and baroclinic instability of the mean flow. The energy input is therefore mostly on scales varying from 50 to 300 km, where energy and enstrophy fluxes can both exist at the same wave number. Several factors, such as the presence of coherent structures (Maltrud and Vallis, 1991) or frontogenesis (Andrews and Hoskins, 1978), have been shown to alter the spectra and may be responsible for the fact that the observed and modeled slopes deviate from the theoretical  $k^{-5}$ .

The spatial variation of spectral slopes from  $k^{-4}$  in the highly energetic areas to  $k^{-2}$  in weakly energetic ones is a more controversial topic. LT suggests that this variation reflects forcing dynamics, with the mesoscale variability in the eastern domain dominated by direct wind forcing and interaction with topography, resulting not only in the flattening of the spectra but also in its red character at low wave numbers. The hypothesis that fluctuations of the wind forcing can generate turbulence in the open ocean is supported by numerical experiments performed by Treguier and Hua (1987), who found significant nonlinear transfer to shorter length scales of the energy input by the winds. In numerical simulations of an unstable baroclinic jet, (Halliwell et al., 1998) found that the steep spectral slopes predicted for geostrophic turbulence were flattened

when stochastic wind forcing was added to the simulation. Furthermore, the ageostrophic variability of the mixed layer should increase the energy levels at higher wave number, making the spectra whiter in this region.

On the other hand, based on the analysis of their medium resolution numerical simulation, SB argue that at very low energy levels, such as in the eastern North Atlantic, the observed flattening reflects the contamination of the ocean signal by measurement noise. Data from TOPEX/Poseidon (of greater accuracy when compared to GEOSAT) were analyzed by Stammer (1997), who also found a departure from the slopes predicted by the geostrophic turbulence theory at high wave numbers. Assuming that the energy at these scales is dominated by noise, Stammer (1997) determined an empirical function for noise spectrum. Correcting the sea surface height spectra for the noise represented in this way, an approximate  $k^{-4}$  slope was obtained for all extratropical latitudes. Based on this result and on the observed correlation between the length scales of the eddy field and the first baroclinic Rossby radius of deformation, Stammer (1997) then suggests that baroclinic instability is the major source for SSH variability at all latitudes, even in the absence of strong mean oceanic currents. This idea was further explored in Stammer (1998) by analysis of the eddy time scales in the same data set.

Analyzing TOPEX/Poseidon data for the subpolar North Atlantic, White and Heywood (1995) observed that seasonal variations in the eddy field in low-energy areas are well correlated to the wind stress. White and Heywood (1995) suggest that direct wind forcing, as opposed to baroclinic instabilities, is the dominant mechanism for the eddy generation in these areas. A recent analysis (Hargrove, 1998) of altimeter spectra derived from TOPEX/Poseidon for the Pacific Ocean shows the same spectral flattening as observed in the Atlantic. According to Hargrove (1998), this flattening is not a consequence of measurement errors. When these spectra are computed for different periods of the year, they also exhibit a seasonal variation at higher wave number, with more energy during the winter season.

As in SB, the fine-mesh simulation with MICOM does not exhibit the observed geographic variability

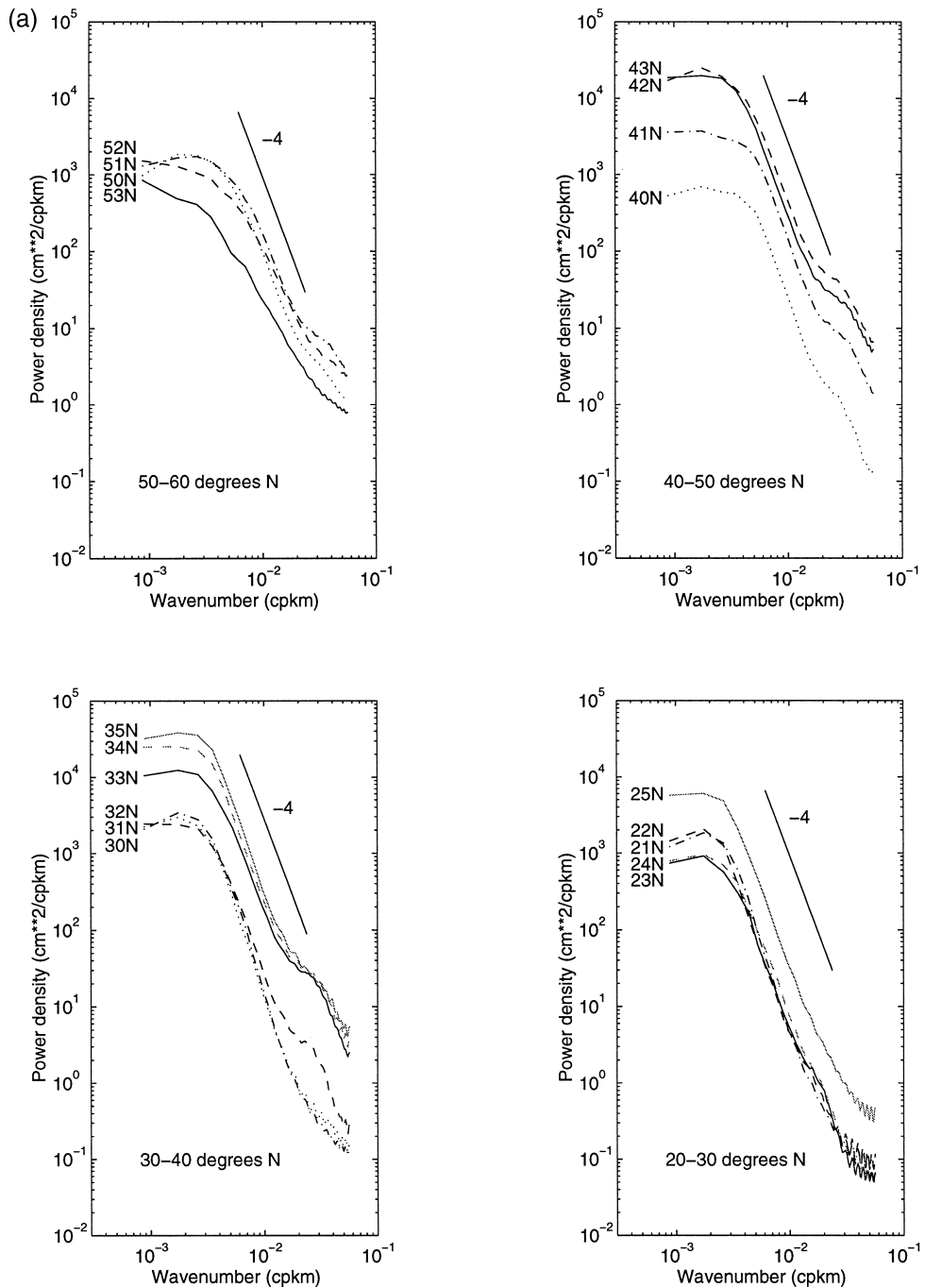


Fig. 7. (a) Sea surface height variability spectra for latitudes from: 50 to 60°N (upper left), 40 to 50°N (upper right), 30 to 40°N (lower left), and 20 to 30°N (lower right). (b) Sea surface height variability spectra for latitudes from: 10 to 20°N (upper left), 0 to 10°N (upper right), 10 to 0°S (lower left), and 20 to 10°S (lower right).

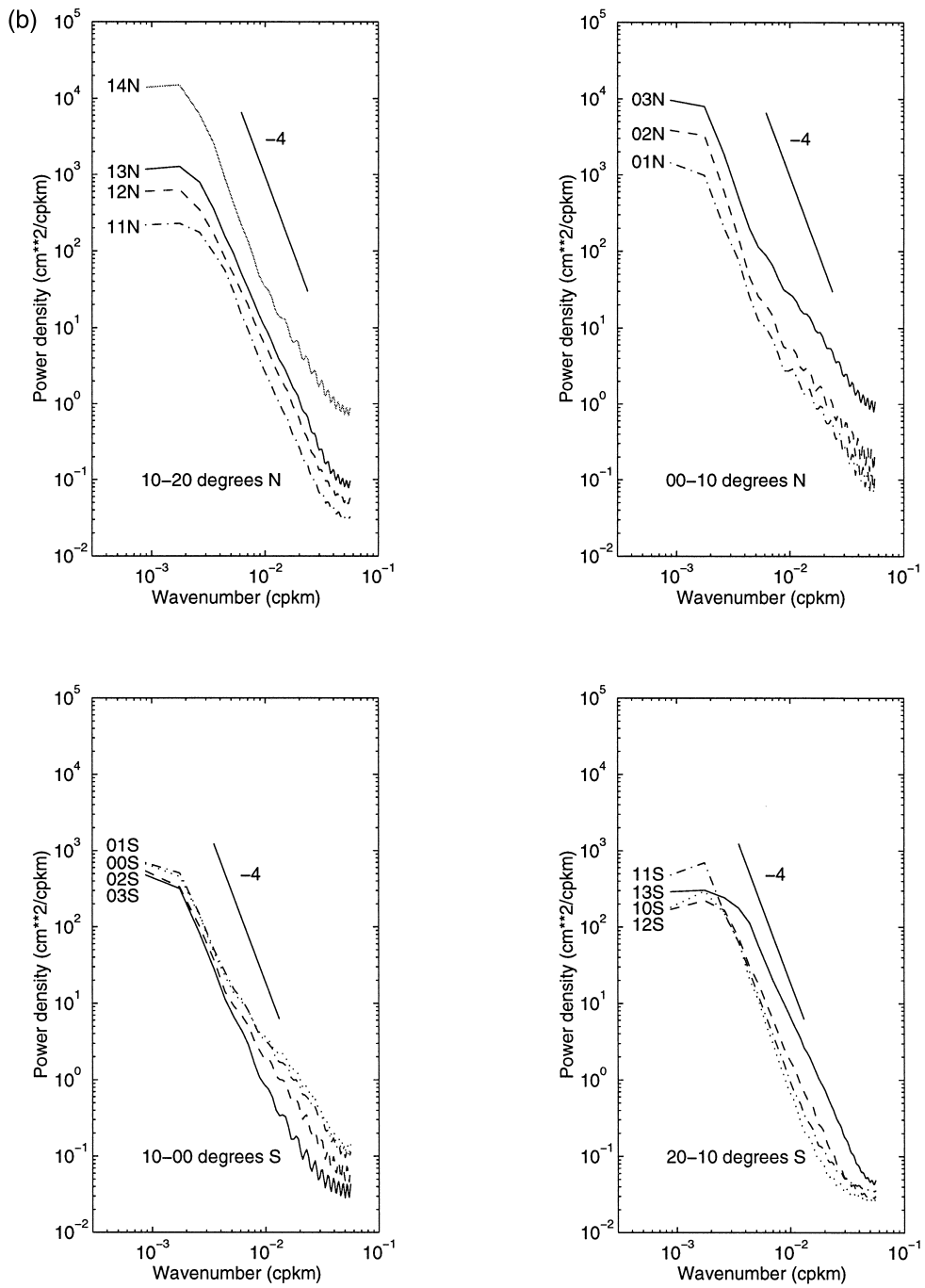


Fig. 7 (continued).

of spectral slopes, which are close to  $k^{-4}$  in most of the domain. It is uncertain if the somewhat weaker

slopes presented in the subpolar gyre, notably in its western part, reflect the less baroclinic character of

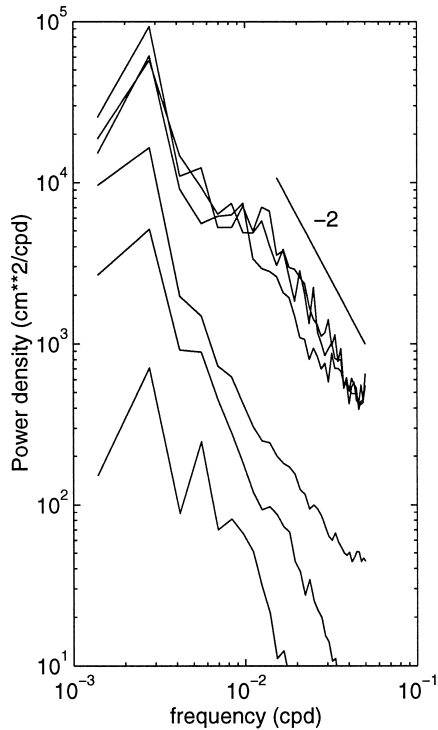


Fig. 8. Frequency spectra. Three lowermost curves computed for boxes 11N, 31N and 51N (in order of increasing energy). Three uppermost curves for the Gulf Stream region (boxes 35N, 34N and 43N).

the flow in these areas, or are somehow related to the grid resolution that marginally resolves the length scales of the eddy field at high latitudes. Model resolution at mid- and low latitudes and a correct Gulf Stream separation do not appear to have a strong impact on the spectral slopes. However, it must be kept in mind that the surface forcings used in this study and in SB are based on monthly climatologies that resolve only the annual cycle and spatial scales on the order of several hundred kilometers. Consequently, mechanisms such as fluctuations in wind forcing on the spatial and temporal scales of atmospheric fronts and eddies, which have been proposed by LT as an explanation for the observed flattening, are not represented in these simulations. The model SSH variability only reflects the contribution from the internal oceanic instabilities. If one accepts the statement of Hargrove (1998) that the measurement errors are not responsible for the spectral flattening, it becomes important to investigate some of the factors that have been put forward as being possibly responsible.

The impact of high frequency wind forcing is presently being investigated in a follow-up experiment, which will be forced by a wind field consisting of a superposition of monthly COADS data, ECMWF (European Center for Medium-Range Weather Fore-

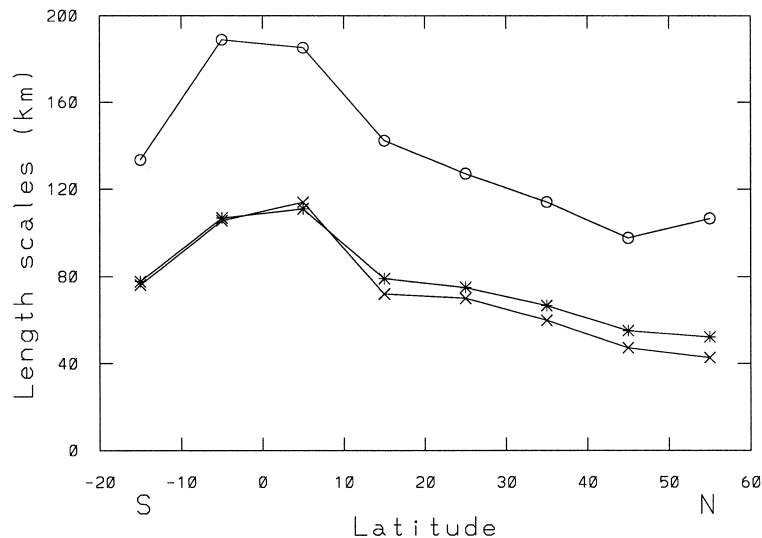


Fig. 9. Latitudinal variation of zonally averaged length scales characteristic of the eddy field:  $L_0$  (open dots),  $L_1$  (stars), and  $L_2$  (crosses).

casting) synoptic scale variability, and high wave number synthetic wind stress variability based on ERS-1 scatterometer statistics (Chin et al., 1998). The frequency and wave number spectra of this data set have been computed (Fig. 11), and significant energy is seen to be present below 180 days and 1000 km, which is not represented in atmospheric climatologies. One must also keep in mind that the energy levels of the model simulation are lower than those derived from the altimeter data. This may be due to the wind forcing as discussed above, the short integration time, lack of vertical resolution in the model mixed layer, or, as recently discussed by the European DYNAMO (1997) project, the use of Laplacian viscosity (rather than biharmonic). These

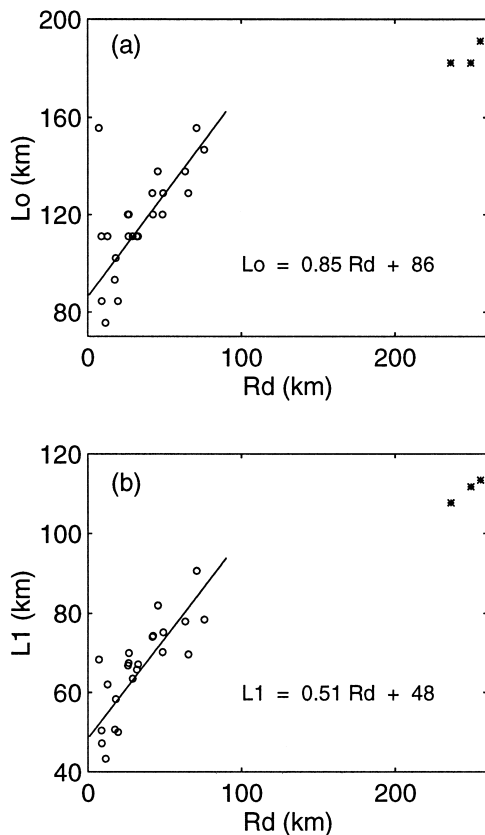


Fig. 10. Scatter plot of length scales of the eddy field against the Rossby radius of deformation: (a)  $L_0$  and (b)  $L_1$ . Dots represent boxes located northward of  $10^\circ\text{N}$ . Stars represent boxes located southward of  $10^\circ\text{N}$ , and for which the linear relationship between the length scales and the Rossby radius is no longer valid.

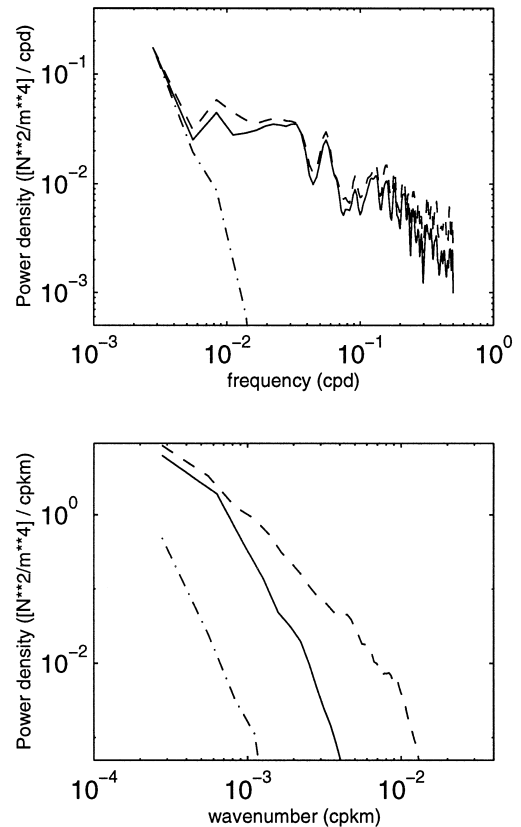


Fig. 11. Frequency (upper panel) and wave number (lower panel) spectra of the zonal component of the wind stress in the North Atlantic at  $38^\circ\text{N}$ . The energy of COADS monthly climatology (dash-dot lines) is mostly in the annual and semi-annual harmonics. These two harmonics and the annual mean are removed from daily ECMWF wind stress and replaced with COADS to produce a stress field (solid lines) which has much greater energy at the wave numbers and frequencies of atmospheric synoptic variability. This field was then supplemented with synthetic atmospheric mesoscale variability that is consistent with ERS-1 scatterometer statistics to produce a final wind stress product (dash lines) having realistic energy from basin-scale to 100 km spatially while retaining the long time scale properties of the COADS climatology.

aspects are presently being investigated in the follow-up experiment.

### Acknowledgements

The authors wish to thank Z. Garraffo for providing the model data and some of the analyses. Our thanks go also to A. Sawdey and M. O'Keefe for their help with the numerical code and to L. Smith

for improving the text. Support was provided by the National Science Foundation through Grant OCE-92-06643 and by the Office of Naval Research under contract N00014-93-1-0404. A.M. Paiva was supported by a fellowship from the Brazilian Research Council (CNPq). J.T. Hargrove was supported by a NASA Earth System Science Fellowship.

## References

- Andrews, D.G., Hoskins, B.J., 1978. Energy spectra predicted by semi-geostrophic theories of frontogenesis. *J. Atmos. Sci.* 35, 509–512.
- Blayo, E., Verron, J., Molines, J.M., Testard, L., 1996. Monitoring the gulf stream path using GEOSAT and TOPEX/Poseidon altimetric data assimilated into a model of ocean circulation. *J. Mar. Sys.* 8, 73–89.
- Bleck, R., Chassignet, E., 1994. Simulating the oceanic circulation with isopycnic-coordinate models. In: Majundar, S.K. (Ed.), *The Oceans: Physical–Chemical Dynamics and Human Impact*. pp. 17–39.
- Bleck, R., Rooth, C., Hu, D., Smith, L.T., 1992. Salinity-driven thermocline transients in a wind- and thermohaline-forced isopycnic coordinate model of the North Atlantic. *J. Phys. Oceanogr.* 22 (12), 1486–1505.
- Bleck, R., Dean, S., O’Keefe, M., Sawdey, A., Numrich, R.W., 1995. A comparison of data-parallel and message-passing versions of the Miami Isopycnic Coordinate Ocean Model (MICOM). *Parallel Computing* 21, 1695–1720.
- Chao, Y., Fu, L.L., 1996. A comparison between TOPEX/Poseidon data and a global ocean general circulation model during 1992–1993. *J. Geophys. Res.* 100 (C12), 24965–24976.
- Chao, Y., Gangopadhyay, A., Bryan, F.O., Holland, W.R., 1996. Modeling the Gulf Stream system: how far from reality. *Geophys. Res. Lett.* 23, 3155–3158.
- Charney, J.G., 1971. Geostrophic turbulence. *J. Atmos. Sci.* 28, 1087–1095.
- Chassignet, E.P., Smith, L.T., Bleck, R., Bryan, F.O., 1996. A model comparison: numerical simulations of the North Atlantic oceanic circulation in depth and isopycnic coordinates. *J. Phys. Oceanogr.* 26 (9), 1849–1867.
- Chin, T.M., Millif, R.F., Large, W.G., 1998. Basin-scale, high-wave number sea-surface wind fields from a multiresolution analysis of scatterometer data. *J. Atmos. Ocn. Tech.*, In press.
- da Silva, A.M., Young, C.C., Levitus, S., 1994. Atlas of surface marine data 1994. Technical Report. National Oceanic and Atmospheric Administration.
- DYNAMO, 1997. Dynamics of North Atlantic models: simulation and assimilation with high-resolution models. Technical Report. Institut für Meereskunde, 334 pp.
- Emery, W.J., Lee, W.G., Maggard, L., 1984. Geographic and seasonal distributions of Brunt–Väisälä frequency and Rossby radii in the North Pacific and North Atlantic. *J. Phys. Oceanogr.* 14, 294–317.
- Forbes, C., Leaman, K., Olson, D., Brown, O., 1993. Eddy and wave dynamics in the South Atlantic as diagnosed from GEOSAT altimeter data. *J. Geophys. Res.* 98 (C7), 12297–12314.
- Fu, L.L., 1983. On the wave number spectrum of oceanic mesoscale variability observed by SEASAT altimeter. *J. Geophys. Res.* 88 (C7), 4331–4341.
- Halliwell, G.R., Olson, D.B., Peng, G., 1998. Evolution of beta-plane turbulence in subtropical gyres due to baroclinic instabilities and stochastic atmospheric forcing. Submitted to *Dyn. Atmos. Oc.*
- Hargrove, J.T., 1998. Zonal variability of eddy energy from TOPEX/Poseidon altimetry in the mid-latitude North Pacific Ocean. Manuscript in preparation.
- Hua, B.L., Haidvogel, D.B., 1986. Numerical simulations of the vertical structure of quasi-geostrophic turbulence. *J. Atmos. Sci.* 43 (23), 2923–2936.
- Kraichnan, R.H., 1967. Inertial ranges in two-dimensional turbulence. *Phys. Fluids* 10 (7), 1417–1423.
- Le Traon, P.Y., 1993. Comments on ‘Mesoscale variability in the Atlantic Ocean from GEOSAT altimeter and WOCE high-resolution numerical modeling’. *J. Phys. Oceanogr.* 22, 2729–2732.
- Le Traon, P.Y., Rouquet, M.C., Boissier, C., 1990. Spatial scales of mesoscale variability in the North Atlantic as deduced from GEOSAT data. *J. Geophys. Res.* 95 (C11), 20267–20285.
- Levitus, S., 1982. Climatological atlas of the world ocean. Technical Report. NOAA.
- Lilly, D.K., 1969. Numerical simulations of two-dimensional turbulence. *Phys. Fluids Suppl. II*, 240–249.
- Maltrud, M.E., Vallis, G.K., 1991. Energy spectra and coherent structures in forced two-dimensional and beta-plane turbulence. *J. Fluid Mech.* 228, 321–342.
- Özgökmen, T.M., Chassignet, E.P., Paiva, A.M., 1997. Impact of wind forcing, bottom topography, and inertia on mid-latitude jet separation in a quasi-geostrophic model. *J. Phys. Oceanogr.* 27, 2460–2476.
- Smith, R.D., Maltrud, M.E., Hecht, M.W., Bryan, F.O., 1998. Numerical simulation of North Atlantic Ocean at 1/10°, preprint.
- Stammer, D., 1997. Global characteristics of ocean variability estimated from regional TOPEX/Poseidon altimeter measurements. *J. Phys. Oceanogr.* 27 (8), 1743–1769.
- Stammer, D., 1998. On eddy characteristics, eddy transports, and mean flow properties. *J. Phys. Oceanogr.* 28 (4), 729–739.
- Stammer, D., Böning, C., 1993. Mesoscale variability in the Atlantic Ocean from GEOSAT altimeter and WOCE high-resolution numerical modeling. *J. Phys. Oceanogr.* 22, 732–752.
- Stammer, D., Böning, C.W., 1996. Generation and distribution of mesoscale eddies in the North Atlantic Ocean. In: Borntraeger, G. (Ed.), *The Warmwatersphere of the North Atlantic Ocean*. Krauss, W.
- Treguier, A.M., Hua, B.L., 1987. Oceanic quasi-geostrophic turbulence forced by stochastic wind fluctuations. *J. Phys. Oceanogr.* 17, 397–411.
- White, M.A., Heywood, K.J., 1995. Seasonal and interannual changes in the North Atlantic subpolar gyre from GEOSAT and TOPEX/Poseidon altimetry. *J. Geophys. Res.* 100 (C12), 24931–24942.